Active Image Formation in Lasers[†]

Abstract: An optical cavity is described in which the modes are determined as stationary states of the diffraction-limited object/image transformation of classical optics; these modes are selected by the insertion of controls into the optical cavity and lead to field distributions which image these controls. When the cavity is driven by an active medium, laser oscillation can occur, and this is discussed in terms of the coupled mode equations used by Wagner and Birnbaum in their theory of quantum oscillation in a multimode cavity. Some properties of these modes in the limits of small and large optical aperture are described and illustrated with experiments using the helium-neon gas laser.

1. Introduction

It was shown by Townes and Schawlow in 1958 that sustained stimulated emission of light could be obtained if light waves were multiply reflected within an optical cavity so that the resultant high-energy-density standing waves could be amplified by an active medium. They also demonstrated that this emission, or laser oscillation, would primarily build up into a single optical mode or fundamental resonance of the confining optical cavity, specifically into that mode which possessed the highest Q or quality factor and for which the confined optical energy density would be greatest. Wagner and Birnbaum later gave a more detailed description of the process of mode condensation as a selection of the most favoured mode for oscillation from the very large number of possible modes in the essentially multimode optical cavity.

Subsequent investigations have shown the general occurrence of mode condensation in laser oscillation, but it has been recognized that this selection is effective only very near a gain threshold. As this threshold is exceeded, many new modes can appear unless the optical cavity is specifically designed to suppress these modes—their growth reduces the efficiency of the laser with respect to the generation of maximum energy into a single mode. Such secondary modes have been attributed to crystalline imperfections in solid state lasers, to inhomogeneous line broadening in gas lasers, generally to

the effect of optical imperfections and mirror misalignment of the laser cavity, and also to nonuniform excitation of the active medium.

In the present paper an optical cavity, Fig. 1, is employed in which many modes of equal O but with varying field distributions can be excited in laser oscillation; it will be shown that these modes may be described in terms of the diffraction-limited object/image transformation of classical optics. Generally, the laser oscillation in this cavity corresponds to a roughly uniform but multimode illumination over the field of the confining mirrors but this may later be perturbed by the introduction of objects or masks into the cavity at a mirror surface, locally destroying the mirror reflectivity at this location. It is found that the resultant field distribution in laser oscillation can be projected from the cavity and refocussed by conventional optical elements to form images of these objects. It is in this sense that the title of this paper refers to active image formation.

Figures 3-5 (pp. 36-37) and others illustrate images formed in this way and make it apparent that the inserted objects do not merely suppress certain modes of the optical cavity in the regions where the object absorbs or scatters energy but, rather, the modes excited in laser oscillation conform to and map the edge detail of the objects or masks with fidelity and with high contrast. Further, this image definition increases with the laser gain as an increasing number of modes oscillate simultaneously. Thus, the active imaging discussed in this paper depends upon the multimode oscillation that

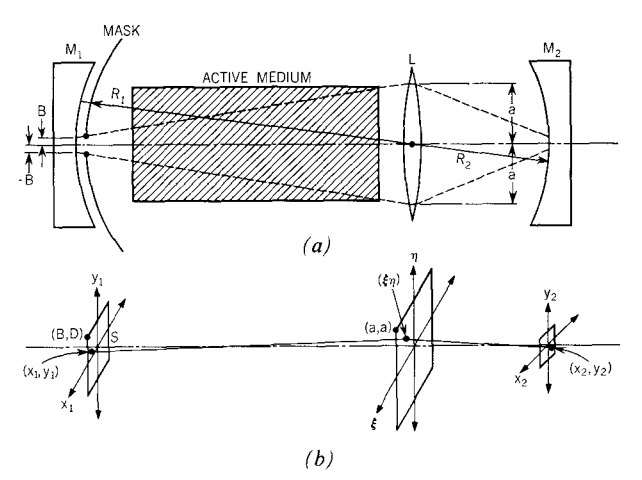
^{*} Present address: Hawkes Avenue, Ossining, New York. †This work was performed when the author was a member of the staff of the IBM Research Division, Yorktown Heights, N. Y.

builds up into contoured high reflectivity areas as these modes are driven by the active medium.

Image formation of this type is, of course, quite different from the conventional, passive image formation obtained with a simple lens. In this last, each point of an illuminated object serves as a source for waves that are focussed by the lens into overlapping diffraction patterns in the image plane, producing the usual diffraction-limited resolution. Apart from this spreading, however, there is a fixed ratio between the intensity of the light radiated from the source points to the intensity of these points in the image. In contrast, in active imaging the intensity in the image depends upon the number and the field distribution of modes that oscillate into the given image area. The modes may each have different optical frequencies and different intensities, with the latter depending both upon the diffraction loss of each mode and upon the competition of these modes within the active medium of the laser for the gain-producing population inversion. Essentially, therefore, this process must be described in terms of the properties of the allowed modes of the system together with the coupling and interaction of these modes with the laser active medium. An initial description of this process is attempted in the subsequent sections of this paper.

The basic optical cavity used in this work is shown in Fig. 1, where L represents a simple lens and M₁ and M₂ are high reflectivity mirrors located at object and image positions for the lens L. Within the limits of Fraunhofer diffraction and neglecting optical aberrations in the system (viz., within the approximations implied in Eqs. (8a, 8b) below), it is clear that a source area at one mirror will be transformed into itself by rays that pass through L and are then reflected back through L from the facing

Figure 1 (a) The arrangement of components used in active imaging and (b) the coordinates used in the derivation of the modes of the optical cavity.



mirror. Additionally, to avoid walk-off losses, the orientation and position of the mirror surfaces must be such that each wave advancing against the surface is returned exactly upon itself. This condition is satisfied when, for each of the terminating mirrors, the lens L, considered as an object, is its own conjugate image in the mirror. For spherical mirrors this requires that L be located at a center of curvature of each mirror and that the radii of curvature of the mirrors correspond to the usual object and image distances for imaging by L. The mirrors thus act as field lenses for the lens L. Subject to these conditions, it will be shown in Section 2 that an optical field distribution can be described for this system in terms of eigenfunction solutions of an integral equation that depends upon the shape and size of the high reflectivity surface of one of the terminating mirrors.

This surface is taken here to be defined by an aperture in a mask placed before one mirror, Fig. 1. As the aperture is contracted, it will be shown that there exists a minimum source area which will have a diffraction loss sufficiently low that laser oscillation can occur in a field distribution within the geometric ray boundaries shown as dashed lines in Fig. 1; the dimensions of this limiting area will depend upon the laser gain available within the active medium. It has been found that with high quality optical components there is sufficient gain of the heliumneon gas laser in the visible transition at 6328 Å to allow oscillation to occur for circular source areas with diameters of the order of 2.5 Airy disk diameters for the system. (The Airy disk diameter is here taken as a convenient and conventional measure of the scale of the diffraction spreading produced in the image plane of an aperturelimited objective lens.³) If R is the distance from the objective to the image plane for light of wavelength λ , two Airy dimensions may be defined: a disk diameter, A_d , for diffraction by a circular aperture of radius a,

$$A_d = \frac{1.22\lambda R}{a} = \frac{1.22\lambda}{N.A.},\tag{1}$$

and an Airy width, A_w , for diffraction through one dimensional apertures such as a slit of width w,

$$A_w = \frac{2\lambda R}{w} = \frac{2\lambda}{N.A.}, \qquad (2)$$

where N. A. is the numerical aperture of the objective. Also, in these expressions, R may be taken as the distance from lens L to either mirror M_1 or M_2 , and the diffraction spread at one mirror is thus related to that at the other mirror by the magnification ratio of the optical cavity.

If the source area is only slightly larger than the minimal source area referred to in the preceding paragraph, it is found that higher order modes are simultaneously excited in oscillation if the laser gain is high enough, but that these modes oscillate independently with slightly different

optical frequencies. Further, these single source areas will usually be much smaller than the limiting aperture set by the laser amplifying medium. If multiple source areas exist before one mirror surface, laser oscillation can build up into each of these areas simultaneously, again with multimode oscillation in each such area. The total field distribution is thus highly complicated, but some preliminary experiments have indicated that certain mode interactions, to be discussed in Section 4, cause adjacent and nearly frequency-degenerate optical modes to lock together in optical frequency. This coupling will be shown to have the particularly interesting property that it can be induced when objects that are small compared to an Airy dimension for the system are inserted before one mirror; this can lead to an image field in which the boundaries of the image of the object are formed with a contrast that may be an order of magnitude greater than that which would be predicted by the passive diffraction-limited image formation of conventional optics. This process is discussed in Section 4, under the descriptive heading "Super-resolution."

2. The diffraction transformation

For simplicity it will be assumed that the optical system shown in Fig. 1 is of square cross section with uniform gain across the aperture of the active medium. The limiting aperture for imaging will most often be determined by the allowed cross section of the active medium and is taken as having a width and height of dimension 2a. This Section, then, is concerned with the wave field which can exist in the passive optical cavity that is bounded at mirror M₁ by a source area S. The source area may be introduced by a mask with a cut-out to expose a high reflectivity mirror surface with the shape of the source. Further, S will also be taken as rectangular and defined by $-B \le X \le B$ and $-D \le Y \le D$, for the coordinate system shown in Fig. 1. The actual field distributions at the terminating mirrors are related in their size by the lateral magnification, M, of the optical cavity with M = $-R_2/R_1$. It will be useful to use scale normalized "optical coordinates" (x_1, y_1) at the mirror M_1 by the use of the definitions3

$$x_1 = M X_1, y_1 = M Y_1.$$
 (3)

Similar "optical coordinates" may be defined for the source area S,

$$b = MB, \qquad d = MD. \tag{4}$$

It will also be assumed in the following that the use of Fraunhofer diffraction provides a sufficiently accurate formulation for the derivation of the wave field, and this implies that the path length s from a point (x_1, y_1) at mirror M_1 through lens L at (ξ, η) to the point (x_2, y_2) at

mirror M2 is very well approximated by the expansion

$$s = 2 \left\lceil R - \frac{(x_2 - x_1)\xi + (y_2 - y_1)\eta}{R} \right\rceil.$$
 (5)

For a given wave function $U_1(x_1, y_1)$ on M_1 the field propagating away from the mirror may be determined from the Huygens-Fresnel integral. (We note parenthetically that only a monochromatic field is considered here with the time periodic factor $e^{-i\omega t}$ being suppressed, as is customary.) The lens (or, as will be seen later, an objective mirror) transforms these waves into diffracted, convergent waves with amplitude $U_2(x_2, y_2)$ on mirror M_2 , and this transformation is represented by the diffraction-limited object/image integral³

$$U_2(x_2, y_2) = \int_{-b}^{b} \int_{-d}^{d} U_1(x_1, y_1) K(x_1, y_1; x_2, y_2) dx_1 dy_1.$$
 (6)

Here, $K(x_1, y_1; x_2, y_2)$ is the transmission function for lens L. This function may be expressed in terms of the pupil function of the lens L, determined by the focussing action of L in forming the image producing wave. Thus, if $G(x_1, y_1; \xi, \eta)$ is the pupil function of the lens, then

$$K(x_1, y_1; x_2, y_2) = \frac{1}{(\lambda R)^2} \int_{-a}^{a} \int_{-a}^{a} G(x_1, y_1; \xi, \eta)$$

$$\cdot e^{(-2\pi i/\lambda R) [(x_2 - x_1)\xi + (y_2 - y_1)\eta]} d\xi d\eta. \tag{7}$$

As noted in Born and Wolf, the phase of G determines the aberration function for lens L and the amplitude of G gives any non-uniformity in the amplitude of the image forming wave due to attenuation in lens L. For a perfect lens, as will be assumed here (i.e., we neglect the aberrations of lens L and any non-uniformity in its amplitude transmission), G may be taken as unity, with the result that $K(x_1, y_1; x_2, y_2)$ is simply

$$K(x_1, y_1; x_2, y_2) = K[(x_2 - x_1), (y_2 - y_1)]$$

$$= \frac{1}{\pi^2} \frac{\sin [(2\pi a/\lambda R)(x_2 - x_1)]}{(x_2 - x_1)}$$

$$\cdot \frac{\sin [(2\pi a/\lambda R)(y_2 - y_1)]}{(y_2 - y_1)}.$$
 (8b)

The first expression, Eq. (8a), indicates the isoplanatic character of the system, i.e. it shows that the transmission through lens L is independent of a specific source point (x_1, y_1) provided that this point lies within the entrance aperture of the laser active medium and lens L.³

It will also be assumed that the field amplitude function $U_1(x_1, y_1)$ is separable in the coordinates x and y so that, according to Eqs. (6) and (8b), $U_2(x_2, y_2)$ is also separable. This assumption leads to a simplification of the problem

in that it can be treated as one-dimensional, the complete solution being understood to be the product of two independent functions of the type discussed below. Then from Eqs. (6) and (8b)

 $U_2(x_2)$

$$= \frac{1}{\pi} \int_{-b}^{b} U_{1}(x_{1}) \frac{\sin \left[(2\pi a/\lambda R)(x_{2} - x_{1}) \right]}{(x_{2} - x_{1})} dx_{1}. \tag{9}$$

The shape and orientation of the mirrors M_1 and M_2 ensure that the points (x_1, y_1) and (x_2, y_2) lie on a common diameter centered on the lens L, and thus that the reflected wave initially returns exactly upon itself towards the mirror M_1 , in accordance with a second transformation of the type of Eq. (9). The following expression represents the wave function $U_1^r(x_1)$ of the returned wave:

$$U_1^r(x_1) = \frac{1}{\pi^2} \int_{-b}^{b} \int_{S_2} U_1(x_1') \frac{\sin \left[(2\pi a/\lambda R)(x_2 - x_1') \right]}{(x_2 - x_1')} \cdot \frac{\sin \left[(2\pi a/\lambda R)(x_1 - x_2) \right]}{(x_1 - x_2)} dx_1' dx_2, \quad (10)$$

where S_2 denotes the aperture at mirror M_2 . In general, only one mask or limiting shape S will be inserted into the cavity and S_2 will be the full clear area of M_2 ; physically, the field distribution $U_2(x_2)$ will differ from that of $U_1(x_1)$ only by the limited-diffraction spreading at the edges of the image. It is thus a good approximation to take the limits of the integral of Eq. (10) for S_2 as $-\infty \le x_2 \le \infty$ and Eq. (10) simplifies to

 $U_1^r(x_1)$

$$= \frac{1}{\pi} \int_{-b}^{b} U_1(x_1') \frac{\sin \left[(2\pi a/\lambda R)(x_1 - x_1') \right]}{(x_1 - x_1')} dx_1'. \tag{11}$$

If the mask defining the source area S is close to the surface of mirror M_1 , $U_1'(x_1)$ is a source amplitude for a further reflection through the system provided that $U_1'(x_1)$ is now limited to be zero for $|x_1| \geq b$. After many reflections, it may be assumed that a stationary diffraction field is established with the returned wave amplitude taken as proportional to that of the source wave. Thus, if σ is a constant with $|\sigma| \leq 1$, the relation

$$U_1^r(x_1) = \sigma U_1(x_1)$$
, defined for $-b \le x_1 \le b$, (12)

leads to the basic integral equation

 $\sigma U_1(x_1)$

$$= \frac{1}{\pi} \int_{-b}^{b} U_{1}(x_{1}') \frac{\sin \left[(2\pi a/\lambda R)(x_{1} - x_{1}') \right]}{(x_{1} - x_{1}')} dx'.$$
 (13)

Several authors have identified the modes of an optical cavity as solutions of an integral equation that may be derived from the statements of (12) and (6), with $K(x_1, x'_1)$

a kernel chosen for a particular cavity, e.g. Fabry-Perot, confocal, or concentric.4,5,6,7 In particular, Eq. (13) may be derived with the special kernel of Eq. (8b) as a result of two successive Fraunhofer diffractions of the type used by Boyd and Gordon in their discussion of the confocal cavity.⁵ The present derivation of Eq. (13), however, has emphasized the connection of such an integral equation with the diffraction-limited object/image transformation, Eq. (6); physically, the cavity of Fig. 1 is defined with two mirrors and a lens (or, equivalently, with three mirror surfaces, one of which acts as an objective for imaging) and this differs from the two mirror systems of the previous authors. The aperture radius, a, appears within the kernel of Eq. (13) and determines the diffraction spread due to the multiple imaging of the source. The isoplanatic condition Eq. (8a) indicates that the spatial orientation of the mode or modes defined by Eq. (13) with respect to the axis of the optical cavity is independent of the location of the mask opening, $-b \le x_1 \le b$, over the optical field at M₁.

Slepian and Pollack have shown that a complete set of real ortho-normal solutions of the integral equation Eq. (13) exist. These may be ordered in terms of eigenvalues of Eq. (13) which are found to be real and non-degenerate. Both the functional form and the eigenvalues depend upon the source width and the numerical aperture of the imaging system. The eigenfunctions will be designated as $U_m^e(x)$, with

$$c = \frac{2\pi b}{A_m},\tag{14}$$

and $m (m = 0, 1, 2, \cdots)$, denoting the order of the solution and also expressing the number of nodes of the *m*-th eigenfunction. The corresponding eigenvalues, σ_m , represent the fraction of the energy carried by the *m*-th mode which is returned to the source area:

$$\sigma_m = \int_{-b}^b \left[U_m^c(x) \right]^2 dx. \tag{15}$$

By Eq. (13), σ_m is related to the decrease in the field amplitude, so that the total diffraction loss, α_D , is given by

$$\alpha_D = 1 - \sigma_m^2. \tag{16}$$

It is shown by Slepian and Pollak that the eigenfunctions are prolate spheroidal wave functions defined for a specified c.

The eigenvalues have the important property that they are nearly degenerate and of low loss to order $m \approx 2c/\pi$ and above this order have large and rapidly increasing loss. The one-dimensional Airy width, A_w , of Eq. (2), provides a convenient scale for this loss, and, roughly, the number of low loss functions is $(4b/A_w)$, or twice the number of Airy widths allowed in S.

For a given source dimension a lowest order eigen-

function can be obtained in laser oscillation by reducing the laser gain to a minimum threshold, or, alternatively, by reducing the lens aperture 2a by means of an iris diaphragm so as to increase the diffraction loss. At higher gain, however, a number of these modes oscillate simultaneously within the single S aperture. The kinetic reasons for this will be discussed in Section 3, but the main result is that a given source shows a nearly uniformly illuminated field due to the laser oscillation. Further, because the different modes do not generally have quite the same frequency, the illumination represents an incoherent superposition of spatially coherent functions. It must also be noted that the restriction to rectangular apertures is entirely artificial-circles, triangles, and "starfish" shapes are also actively imaged and the associated fields may be considered as a superposition of the eigenfunctions of Slepian and Pollak, or alternatively as eigenfunctions of a modified source area in the imaging optical cavity. It is true, of course, that the lowest order field distributions of high diffraction loss figures, as the "starfish," do not represent uniform illumination of the figure, especially in the arm detail, until the highest laser gains are achieved. For these reasons, it is emphasized that quantitative estimates of diffraction loss, taken from the one-dimensional solutions of Slepian and Pollak, are valid only for the rectangular aperture considered above.

The product of two eigenfunctions, one each for the independent x- and y-directions, thus gives the transverse spatial dependence of the wave field of the distinct modes at the source area S of the optical cavity. The full spatial dependence as this wave propagates into the active medium may be obtained straightforwardly from the diffraction integral. It is an important property of the prolate spheroidal functions that they are their own Fourier transforms, except for a scale factor, so that the transverse dependence of the field is preserved along the axis of a given mode. The field intensity will, however, vary with distance from source area S.

In the formation of standing waves due to multiple reflections within the cavity the round-trip phase change must be a multiple of 2π and the full spatial field dependence of the eigenfunctions is obtained by multiplying the eigenfunctions of Slepian and Pollak by the function $\sin \pi qz$ with z measured along the axis of the mode that also passes through the center of the lens L. These modes are then designated, following Boyd and Gordon, as TEM_{mnq} with the integer q determined by the resonance condition⁵

$$2\pi q = 4 \left| \left[\frac{\pi}{2} + \frac{\pi}{2} \left(m + n \right) \right] \left[1 + \frac{4\Delta}{\pi R} \right] - \frac{2\pi R}{\lambda} \right|. \quad (17)$$

Here, λ is the free space wavelength and Δ , with $\Delta \ll R$, is the deviation of the actual lens-to-mirror "optical separation" from the value for which the center of lens L

coincides with the center of curvature of the mirror. The phase changes for the various modes expressed by the right hand side of Eq. (17) follow directly from an evaluation of the diffraction integral in propagation from the source S through the lens L, and are taken from Boyd and Gordon. Equation (17) may be expressed as a wavelength condition for resonance of the optical cavity,

$$\frac{4R}{\lambda} = q + (1 + m + n) \left(1 + \frac{4\Delta}{\pi R} \right). \tag{18}$$

If Δ is adjusted to be zero, Eq. (18) can be satisfied by a number of different modes of the same optical frequency for which the integer sum on the right-hand side of Eq. (18) is a constant; in turn, the transverse modes of a given frequency with different m and/or n will have noncoincident nodes and antinodes in the energy density. The field distributions of the modes are, thus orthogonal in both their transverse eigenfunctions and their axial field dependence; as is discussed in Section 3, this indicates these modes can be excited as independent modes in laser oscillation.

The frequency degeneracy is removed for a nonvanishing Δ , and Δ is adjusted experimentally by changing the separation of one of the terminal mirrors of the optical cavity from the objective, L. For Δ sufficiently small, Eq. (18) predicts low-frequency beats (i.e. difference frequencies of the order of 50 to 100 kilocycles) between modes of different transverse symmetries that are excited in oscillation in the cavity. Further, the laser beam projected from the cavity can be refocused upon a screen to provide an image of the source area and the field distribution can be scanned by a detector. When the laser gain is adjusted so that only two transverse modes of a single source area oscillate simultaneously, the amplitude of the low frequency beat between the optical modes varies across the image field as the product of the field intensities of the contributing modes. This provides a technique for testing the predictions of this theory. Experimentally, both the beats and the distribution of the beat note intensity across the field of the image were observed and were in good agreement with all the predictions indicated above. A limit to these observations was set, however, by the frequency stability of the beat which was of the order of 20 to 30 kc/sec and which reflected the high vibrational environment of the apparatus. The "optical length" of the cavity depends not only upon the spacing of the mirrors and the lens but also upon the index of refraction of the active medium, as has been noted by Bennett in his discussion of frequency pulling in a gas laser.¹⁰ In the present experiments, the frequency of the beat was a function of the gain of the laser and could be varied by changing the discharge path length within the laser tube. The shift in the beat frequency is then interpreted as a change in the optical length of Δ .

Some further properties of this system would be expected, but have not, at present, been examined theoretically. These include the dependence of the diffraction loss upon the spacing deviation Δ , and also the dependence of the loss upon a physical separation of the mask defining the source area from its adjacent mirror, i.e. M_1 in Figure 1. In the experiments, these factors were not dominant in the sense that the mirror spacings or the mask location required critical adjustment but this undoubtedly reflects the great depth of optical field that is represented by the very large f-number of the gas laser tube (f/200) used in the present work.

The eigenvalues and thus the diffraction loss for a given mode require numerical evaluation for each aperture value, or c-number as given by Eq. (14). Some estimates may be made, however, from the table of eigenvalues given in Slepian and Pollak. A one-dimensional aperture slightly more than two Airy widths wide would admit three eigenfunctions with diffraction loss less than 1% and a square aperture of the same width would admit nine independent functions with diffraction loss also less than 1%. There is sufficient gain in the helium-neon gas laser in the visible transition to overcome this loss, and experimentally, simultaneous oscillation in a number of nearly frequency degenerate modes was observed for an aperture of this type. As reported above, this number could be reduced to 2 or 3 by reducing the laser gain.

A particular imaging system that is simpler than that of Fig. 1 is the ordinary confocal cavity of Fig. 2. Here mirror M2 acts as an objective for the focussing of source areas at M1; by the use of a half mask to form the source area S the unobstructed half of the high reflectivity mirror M₁ is available for the conjugate image of S, S', in M₁. This arrangement, which was used in many of the experiments reported in this paper, is also useful for demonstrating the physical nature of the diffraction loss calculated from the eigenvalues of Eq. (13) as a truncation by the source cutout S of the diffracted wave returned to M₁. Lens L₁ of Fig. 2 is of large aperture and images both the source area S and its conjugate image upon the screen. The boundary of S is sharply defined in the direct image whereas the boundary of the conjugate image is shaded due to the diffraction in the imaging from M2. The diffraction spreading is maintained in the second transit from S' back to the mask defining S, as in the derivation of Eq. (11), and results in a bright illumination of the edge of the mask cutout where the light is absorbed or scattered.

Alternatively, a lens L_2 may be placed behind the mirror M_2 and used to project and re-image S and S' upon a screen. In this arrangement both images are diffraction limited by the effective aperture of the laser active medium. Figures 3–5 demonstrate this imaging for various masks. In all figures the mirror spacing was 100 cm and the

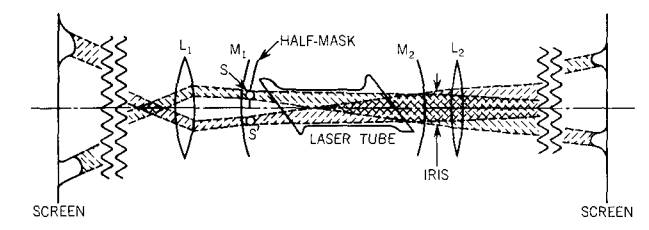


Figure 2 The confocal cavity as a special case of Fig. 1, controlled by means of a half-mask. The aperture in the mask may be re-imaged from the laser output beam from either of the partially transmitting mirrors.

Figure 3 Simultaneous oscillation of the laser into a number of modes defined by masks with square cutouts measuring 0.06×0.06 cm.

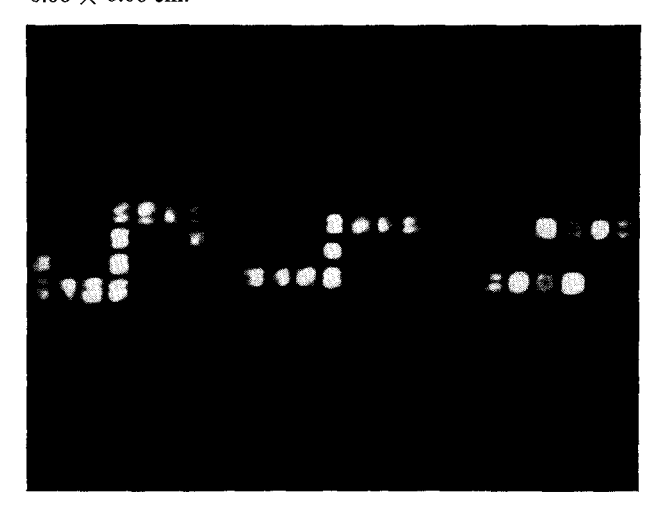
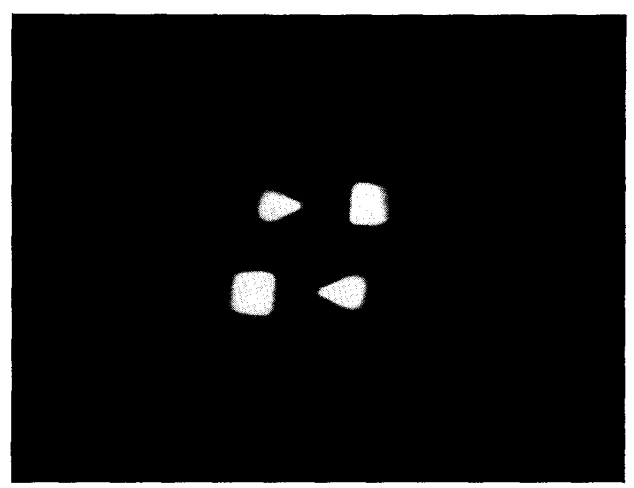


Figure 4 Active imaging of square and triangular cutouts of size near the diffraction limit. The apparatus was that of Fig. 2. The edges of the squares were 0.075 cm; those of the equilateral triangles were 0.09 cm.



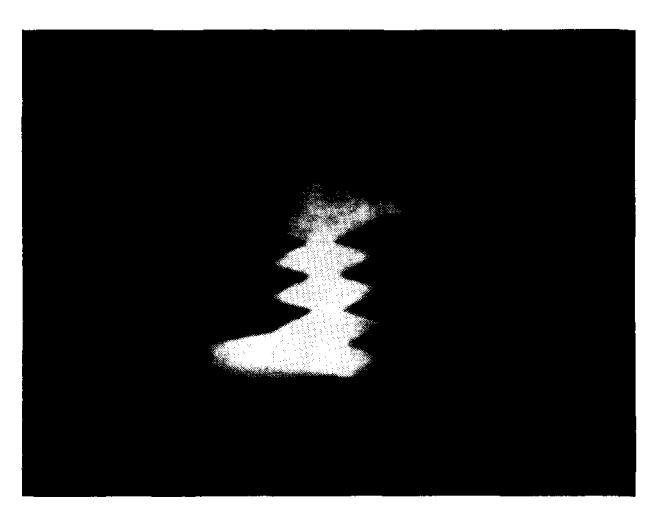


Figure 5 Active imaging of gear teeth with the apparatus of Fig. 2. The sloping edges were 0.12 cm.

effective aperture at M_2 was from 0.5 to 0.6 cm. The insertion of an additional iris behind M_2 and before L_2 did not affect the image quality until it began to intercept the laser output beam, and thus the f-number for this imaging is f/200. For these experiments the Airy width at M_1 for the visible transition is 0.03 cm.

3. Multimode oscillation

It is clear that the process of active image formation depends upon the simultaneous laser oscillation of a number of modes of the optical cavity. The extent to which these fill a given source and their relative intensities determines the degree to which the edge detail of the source area is subsequently imaged after projection of the laser output beam. In this Section the low loss modes of the passive cavity are investigated with respect to their coupling and interaction with the inverted population providing optical gain.

By inspection of Fig. 1 it can be seen that two well separated source areas, S, at M1 will have standing wave fields that are distinct at M₁ but increasingly overlap as they approach the lens L. If the active medium existed only at or very near the surface of M1 the fields of the area S would be wholly separate in the active medium and the oscillation would be that of independent lasers. In the other extreme, with the active medium located at, very near, or in the lens L, the fields that could build up into source areas located anywhere on M1 would overlap completely at L. All of the allowed modes would then be forced to compete with each other for the available gain and mode condensation would be expected to occur—that is, the suppression of the population inversion with laser oscillation would favor the excitation of a single low-loss mode for the system. This implies that

such mode selection would be extremely critical with respect to perturbations and imperfections in the optical cavity.

The long tubes of gaseous optical masers constitute an extended active medium that nearly uniformly fills the space between a mirror and the lens L. With respect to the spatial extent of modes due to given source areas, however, the optical modes do not fill the active medium uniformly. Although this in itself indicates a source of optical gain that would permit simultaneous oscillation into distinct source areas, it has also been seen that a number of low-loss and frequency-degenerate modes may exist and oscillate independently within a single source area S, even though these exist in essentially the same spatial volume of the active medium.

It will be shown later that two modes with only partially overlapping diffraction fields may couple coherently, locking together in frequency. Nonetheless, orthogonal modes of the cavity may have vanishing coupling of this type and oscillate independently. The physical principles governing the quantum oscillations in a multimode cavity were originally derived by Wagner and Birnbaum and their results may be used to discuss this mode coupling, both by extending their work and by adapting their equations to the gas laser used in the present experiments.²

Wagner and Birnbaum's original paper considered an active medium in which the atoms were fixed in position, and for which the atomic transition providing optical gain had a homogeneously broadened line shape; all the atoms can thus provide gain to those cavity modes with frequency response within this line shape. In the gas laser, on the other hand, the oscillations are driven by an inhomogeneous transition (due to Doppler broadening) and this gives rise to the simultaneous and independent axial mode oscillations observed in these lasers—that is, only those atoms which are Doppler-shifted in frequency by a limited range of velocity components of the atom parallel to a direction of mode propagation can couple to a given cavity resonance. Within this frequency range, however, the very high Q of the optical cavity simplifies this coupling, for the active medium may be taken as homogeneously broadened with respect to the atoms responding within the Doppler-shifted spectral interval.

Each moving atom will thus pass through many standing waves and, if there are a number of different modes overlapping in this region, the atom can couple to each of these. The atomic diffusion length is, however, limited by the lifetime of the transition and may be taken as less than 0.01 cm for the 6328 Å transition of the heliumneon gas laser. Although this dimension is more than one hundred optical wavelengths, it is less than one-tenth of the transverse extent of the modes of the optical cavity in the present experiment (with a one-meter mirror spacing). This indicates that the population inversion is

well averaged over the axial modes, but that the cross-excitation of the transverse optical modes by atomic diffusion may be neglected. These approximations will be made in this paper, so that the probability for stimulated emission of an atom into a mode is taken as depending only upon the transverse dependence of the radiation energy density of the given mode. For this model of the helium-neon laser, the theory of Wagner and Birnbaum may be applied directly.

First, it will be taken that the cavity is defined by a single source area with allowed field distributions given by the TEM_{mnq} modes. Employing the assumptions made above and neglecting frequency factors that reflect the line width of the atomic transition, a basic equation of Wagner and Birnbaum may be written as

$$(-\omega^{2} + \omega_{i}^{2})Q_{i} - i(\omega\gamma_{i} - \omega_{i}^{2}B\langle n(\mathbf{r})f_{i}^{2}\rangle)Q_{i} + i\omega_{i}B\sum_{\substack{k\\k\neq j}}\omega_{k}\langle n(\mathbf{r})f_{i}f_{k}\rangle Q_{k} = F.$$
 (19)

The time-dependent normal coordinates Q_i in Eq. (19) are the mode amplitudes of the TEM_{mnq} modes with j or k corresponding to the (m, n, q) triad; the spatial field dependence is contained in the real functions of position, $f_i(\mathbf{r})$. Equation (19) relates the time-dependent amplitudes of the modes driven by the forcing term F which is due to spontaneous emission, while B is a constant depending upon the dipole moment of the atomic transition, ω is the frequency of the laser oscillation, and ω_i is the resonance frequency of the j-th mode of the passive cavity as determined from Eq. (18). These frequencies are taken as nearly identical, and certainly with a difference frequency much less than that represented by the reciprocal of the atomic life time. Further, $n(\mathbf{r})$ specifies the excess population as a function of position within the active medium. The expressions in the angular brackets in Eq. (19) are integrals over the mode volume V, and express the coupling of the modes to the active medium.

The original paper of Wagner and Birnbaum neglected the spatial dependence of the population inversion as well as the mode cross-coupling indicated in the summed term in Eq. (19). They determined the average population inversion, $\langle n(\mathbf{r}) \rangle$, as a function of the energy in the excited modes in the multimode cavity and stressed the property of mode condensation, i.e. the selection of a single dominant mode in laser oscillation, that was demonstrated through their formalism. Later Statz, Tang, and deMars¹¹ showed that if the spatial dependence of $n(\mathbf{r})$ is included when treating a homogeneously broadened atomic resonance associated with fixed atoms, as in ruby, a number of axial modes could be simultaneously excited, and they estimated the number of these modes as well as

the effect of this mode coupling upon the time-dependent spiking observed in solid state lasers.¹⁰ An approximation similar to that of Statz, Tang, and deMars for the spatial dependence of the population inversion is made in this paper and used in Eq. (19) to indicate the effect of the mode coupling and, also, to show that independent and simultaneous oscillation in transverse modes can occur in the gas laser, even when these are very nearly identical in frequency.

Conservation of energy at the position r may be used to relate the excess population inversion n(r) to the number of photons in each mode of the optical cavity. The number of photons in mode j, N_j , is directly related to the energy of a given mode and to the mode amplitudes, Q_j , for the j-th mode. Thus,²

$$N_i = (\omega_i/\hbar) |Q_i|^2. \tag{20}$$

If \bar{n} is the spatially independent density for uniform excitation of the active medium but with no stimulated emission, D is the probability for spontaneous emission into a single mode, and τ is the effective spontaneous emission lifetime, it follows that

$$n(\mathbf{r}) = \bar{n} - D\tau n(\mathbf{r}) \sum_{i} N_{i} g_{i}^{2}(x, y). \tag{21}$$

The functions $g_i(x, yz)$ primarily express only the transverse spatial dependence of the functions $f_i(\mathbf{r})$ because of the assumption that the population inversion, $n(\mathbf{r})$, is to be averaged over the axial modes. A z-dependence of the g_i functions is then due only to the diffraction spreading along the axis of the j-th mode and it is understood that $|\partial g_i/\partial z| \ll q$. Equation (21) may be written as

$$n(\mathbf{r}) = \frac{\bar{n}}{1 + D\tau \sum_{i} N_{i} g_{i}^{2}}$$
 (22)

The sum in the above properly includes all the modes of the system, but Eq. (22) may be simplified and approximated (1) by including only the oscillating modes for which N_i is large so that for r oscillating modes $1 \le j \le r$, and (2) by assuming that the threshold is not greatly exceeded so that a first power expansion of the denominator is valid; i.e.,

$$n(\mathbf{r}) \approx \bar{n} \left(1 - D\tau \sum_{j=1}^{r} N_j g_j^2\right)$$
 (23)

Insertion of (23) into (19) thus provides a basic equation for determining the field amplitude and distribution in laser oscillation as a function of the pumping level, expressed by \bar{n} , and the mode losses, γ_i . With complete frequency degeneracy and by taking the classical condition for oscillation as a demand that the effective conductance of the system vanish, the coupled mode equations become

$$\left[\frac{\gamma_{i}}{\omega} - B\bar{n} \int_{V} \left(f_{i}^{2} - D\tau \sum_{s=1}^{r} N_{s} f_{i}^{2} g_{s}^{2}\right) dV\right] Q_{i}
+ BD\tau \bar{n} \sum_{\substack{k \ i \neq k}} \left(\sum_{s=1}^{r} N_{s} \int_{V} f_{i} f_{k} g_{s}^{2} dV\right) Q_{k} = 0. \quad (24)$$

When the cross-coupling term (the second integral in Eq. (24)) vanishes, Eq. (24) reduces to the equations of Statz, Tang, and deMars and may be regarded as a set of linear homogeneous equations determining the N_i photon populations. The integral

$$\int_{V} f_i^2 \ dV \tag{25}$$

is the volume of the active medium used by the j-th mode, and the remaining term,

$$BD\tau \bar{n} \sum_{s=1}^{\tau} N_s \int_{V} f_i^2 g_s^2 dV, \qquad (26)$$

represents the effect of photons in various modes in suppressing the gain available in the j-th mode. For Fabry-Perot ruby lasers, Statz, Tang, and deMars were able to evaluate the number, r, of oscillating modes with $N \gg 0$ because the integrals of the type of Eq. (26) were simple and because they could assume that the loss dependence of γ_i originated in the frequency dependence of the homogeneous line shape. 11 For the TEM_{mnq} modes considered here the integrals of Eq. (26) are not simple and the dependence on mode number of the eigenvalues, or equivalently the γ_i , is not given, except by numerical integration for a given aperture. With the approximation that the eigenvalues are unity to the $(4b/A_w)$ -th order and decrease rapidly thereafter, the number of simultaneously oscillating modes in the two dimensional field would be just the square of this number (this follows as the integral of Eq. (26) is roughly independent of j and s, and the r equations of Eq. (24), neglecting cross-coupling, become identical). Also, the intensities of the modes would be approximately equal.

It is clear from Eq. (24), however, that if the cross-coupling integral,

$$\int_{V} f_i f_k g_s^2 \ dV, \tag{27}$$

does not vanish, energy in the k-th mode is effective as a gain in driving the j-th mode; further, in view of the fact that the frequencies are nearly identical, as is here assumed, and assuming perfect alignment for the optical cavity of Fig. 1, such coupling will act on the field amplitudes and result in a coherent superposition of these modes. Eq. (27) may be written more explicity as

$$\int_{V} g_{m,n} g_{m',n'} g_{s,s'}^{2}(\sin q\pi z)(\sin q'\pi z) dx dy dz, \qquad (28)$$

for j = (m, n, q), k = (m', n', q'), and s = (s, s'). If m, m' as well as n, n' are of opposite parity, Eq. (28) will necessarily vanish and such modes cannot, therefore, couple coherently. In view of Eq. (18), certain other terms of Eq. (28) will be very small with respect to the assumption that the population inversion n(r) couples uniformly to the axial modes and that the active medium nearly fills the region between M_1 and L of Fig. 1. The lowest-order even-parity modes which would be expected to show significant coherent coupling are the TEM_{02q} and the TEM_{20q} and the lowest-order odd-parity modes are TEM_{13q} and TEM_{31q} .

The above considerations indicate that with a gaseous active medium in the optical system of Fig. 1 and for a single source area S there will be nearly as many simultaneously oscillating transverse modes of almost the same frequency as are permitted by the gain that can drive the low diffraction loss modes; additionally, there will be a number of modes, separated in frequency by c/4R, with each representing "hole burning" within the Dopplerbroadened line.10 For two or more separated source areas, S, there will be an equivalent multimode oscillation at each area although gain suppression in the common volume of the active medium that is shared by these modes reduces the number of modes oscillating in each area. The latter effect is readily demonstrated experimentally by the use of masks to define several source areas, say S₁ and S₂. If the laser gain is reduced, a condition may be found for which there will be one area, S1, which can be controlled to oscillate in a single transverse mode. If S₁ is now blocked off there will be an increase in intensity in S₂ as well as in the possibility of a greater number of transverse modes oscillating within the aperture S2. This increase provides sharper definition of the shape and edge detail of the aperture S2.

4. "Super-resolution"

So long as the aperture product, c, of Section 2, Eq. (14), is taken as small, permitting only a few modes to be generated in the gas laser, good agreement between the theory and experimental observations of active imaging may be obtained. As the aperture number becomes larger, however, the diffraction loss of a great number of modes becomes insignificant with respect to other loss mechanisms and perturbations within the optical cavity, and a given source area loses control of the mode formation except at edge boundaries where the field is suppressed. We note, for example, that in the limit of large b (or small λ), Eq. (13) becomes a Fourier identity, and thus any regular function $U_1(x_1)$ that vanishes in the neighborhood of the boundary will have low diffraction loss. The coupled equations (Eq. (23)) that determine the field distribution

in oscillation are then primarily sensitive to the variation of the loss parameters, γ_i , of competing modes with respect to optical inhomogeneities, to mirror misalignment, and to spatial variations in the laser gain.

The low gain of the gas laser in the visible transition (about 1%/transit) further limits the effect of apertures in controlling the oscillating field distribution through the diffraction loss, since the latter cannot be greater than this value. While the residual losses in the optical system may be taken to be of the order of 0.1%, this loss is essentially constant for all of the modes of the cavity insofar as it represents a lack of perfect mirror reflectivity and absorption in the windows of the laser discharge tube. Inhomogeneities in the optical components will influence mode selection within apertures of sufficient size such that they represent very small diffraction loss, but it is difficult to estimate the magnitude of these effects. The components used in the present experiments were sufficiently homogeneous so that when the only aperture was that of the laser tube itself the oscillating field distribution was primarily sensitive to gradients in the index of refraction of the air that were induced by speaking quietly near one mirror. This perturbation scrambled the modes of the field distribution, producing rapidly varying and complex patterns; it is cited to indicate the sensitivity of the field distribution in this type of optical cavity to extremely small perturbations. In this connection, it may also be noted that while the cavity of Fig. 1 was extremely critical with respect to mirror alignment, the off-axis imaging of the confocal cavity of Fig. 2, for which the terminating mirrors were automatically aligned by being part of a common mirror surface, was much less sensitive in this respect.

In this Section, the field distributions that may exist in the active imaging system of Fig. 1 will be investigated for the case when multiple source areas S exist at mirror M₁ and also for the limit that M₁ is of large aperture but the field distribution is perturbed by the insertion of small opaque objects into the optical cavity at the mirror M_1 . As the field is established in laser oscillation, it will be partially transmitted through one of the boundary mirrors as the laser output beam and may be subsequently refocused by passive optical elements to define an image of the set of apertures or the object. The definition of detail in this type of image depends critically upon the number of modes and their field distribution and thus upon the effect of the perturbing object in selecting the actual field distribution; it is found experimentally that the field in the image of small objects must in part be regarded as a coherent superposition of modes that extend over a much larger high reflectivity area of the terminating mirror M₁ than is represented by the object size itself. This superposition of modes of low diffraction loss can be regarded as an "image" of an obstructing obstacle at mirror M1.

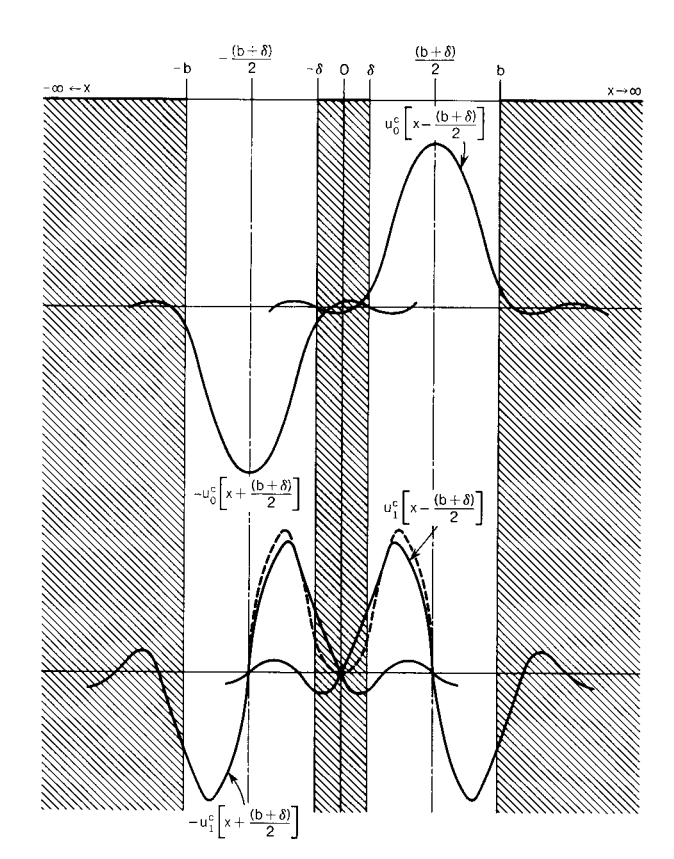


Figure 6 High reflectivity areas at mirror M_1 for $-b \le x \le -\delta$ and $\delta \le x \le b$. This specific example indicates that the coherent superposition of modes of the same order defined for different zones of high reflectivity at mirror M_1 can (1) lead to lower diffraction loss and (2) yield a net field that more sharply defines edge boundaries (here a central obstruction) by the suppression of side lobe radiation.

This property may be illustrated by a specific example of two slits in one-dimensional imaging, Fig. 6.

The two slits are shown in Fig. 6 as high reflectivity areas at mirror M_1 for $-b \le x \le -\delta$ and $\delta \le x \le b$. As shown in Section 2, an ordered set of eigenfunctions and eigenvalues exists for either slit by itself; these sets are defined for each aperture of width $|b-\delta|$. For these functions (cf. Eq. (15)), it will be taken that $c = \pi a(b-\delta)/\lambda R$ with the functions centered upon a central position, $\pm x_0$, within the slit with $x_0 = |(b+\delta)/2|$. In the plane of M_1 the field distribution may be taken as a sum of these functions of a given order, m; viz., as

$$Q_m(x) = a_m^+ U_m^c(x - x_0) + a_m^- U_m^c(x + x_0).$$
 (29)

The function above should satisfy a stationary condition for the double slit similar to that of Eq. (13):

$$\sigma_m Q_m(x) = \int_{M_1} Q_m(x') \frac{\sin \left[\frac{2\pi a}{\lambda R} (x - x') \right]}{\pi (x - x')} dx', \quad (30a)$$

$$= a_{m}^{+} \int_{\delta}^{b} U_{m}^{c}(x' - x_{0}) \frac{\sin \left[\frac{2\pi a}{\lambda R}(x - x' - x_{0})\right]}{\pi(x - x' - x_{0})} dx'$$

$$+ a_{m}^{-} \int_{-b}^{-\delta} U_{m}^{c}(x' + x_{0})$$

$$\cdot \frac{\sin \left[\frac{2\pi a}{\lambda R}(x - x' + x_{0})\right]}{\pi(x - x' + x_{0})} dx'$$

$$+ (a_{m}^{+} + a_{m}^{-}) \int_{\delta}^{b} U_{m}^{c}(x + x_{0})$$

$$\cdot \frac{\sin \left[\frac{2\pi a}{\lambda R}(x - x' + x_{0})\right]}{\pi(x - x' + x_{0})} dx'. \tag{30b}$$

Because the terms $U_m^c(x - x_0)$ are eigenfunctions of the slit of width $(b - \delta)$ with eigenvalues σ_m^c , and because of the symmetry of the present example, the simplest solution may be taken as

$$\sigma_m Q_m(x) = a_m \sigma_m^c \left[U_m^c(x - x_0) - U_m^c(x + x_0) \right]$$
 (31)

for $a_m^+ = -a_m^- = a_m$. The eigenvalue, σ_m , may then be determined by

$$\sigma_m = \frac{\int_{M_1} Q_m^2(x) dx}{\int_{-\infty}^{\infty} Q_m^2(x) dx}.$$
(32)

By substituting (31) into (32), and using the orthonormality of the $U_m^e(x - x_0)$ functions,

$$\sigma_{m} = \frac{\sigma_{m}^{c} - \int_{M_{1}} U_{m}^{c}(x - x_{0}) U_{m}^{c}(x + x_{0}) dx}{1 - \int_{-\infty}^{\infty} U_{m}^{c}(x - x_{0}) U_{m}^{c}(x + x_{0}) dx}.$$
 (33)

The integral in the denominator of Eq. (33) may be shown to be 0 by writing the functions in terms of their integral equation Eq. (13), and by integrating over the transmission functions independently. The integral in the numerator may also be rearranged and expressed as an overlap integral for the functions over the opaque sections of M_1 .

$$\sigma_{m} = \sigma_{m}^{c} + \left[\int_{-\infty}^{-b} + \int_{-\delta}^{\delta} + \int_{b}^{\infty} \right] \cdot \left[U_{m}^{c}(x - x_{0}) U_{m}^{c}(x + x_{0}) \right] dx$$
(34a)
$$= \sigma_{m}^{c} + \int_{-\infty}^{\infty} U_{m}^{c}(x - x_{0}) U_{m}^{c}(x + x_{0}) dx.$$
(34b)

By the definition of Eq. (32), σ_m cannot be greater than 1. Some examples are shown in Fig. 6 for various orders, m, which indicate that for certain values of b and δ , the effect

of the overlap integral of Eq. (34b) is to increase σ_m with respect to the values σ_m^c and that this sum has, therefore, lower diffraction loss than either slit oscillating independently. The effect of the superposition in reducing the diffraction loss at the obstacle, $-\delta \leq x \leq \delta$, by the suppression of the field at the obstacle is also indicated in Fig. 6.

The overlap integral in the numerator of Eq. (33) or in Eq. (34b) is to be compared with that of Eq. (19) where it represented a driving term for the coupling of the mode with amplitude Q_k to that with amplitude Q_i . In the derivation of Eq. (24) it was assumed that only a single source area S existed. The orthogonality of the $U_m^c(x)$ modes then caused the coupling integral

$$B\bar{n} \int_{V} f_{i} f_{k} dV \tag{35}$$

to vanish, so that the only amplitude coupling terms were those written in Eq. (24) and, more explicitly, in Eq. (28). If Eq. (35) is written in terms of the triads j = (m, n, q) and k = (m', n', q') the coupling term, Eq. (35), becomes

$$B\bar{n} \int_{V} g_{m,n} g_{m',n'}(\sin q\pi z)(\sin q'\pi z) dx dy dz, \qquad (36)$$

and it is to be understood that this expression is to be evaluated for modes j and k which only partially overlap, as in the two-slit example.

The effect of, and thus the existence of, such coherent coupling in laser oscillation for adjacent source areas may be demonstrated experimentally by superposition of the laser output beams from the separate source areas and examining the resultant pattern for stationary interference fringes. These fringes are found when the two slit areas are so close to each other (of the order of an Airy width separation) that the diffraction fields of each may be expected to overlap. Additionally, however, when such field distributions are detected and examined for coherent beats in a spectrum analyzer, it is found, at large laser gain, that a number of frequency independent modes are oscillating simultaneously. It is believed that these represent sets of modes of different order, m. From Eq. (36), it is seen that modes with different axial mode numbers q and q' will not couple significantly provided the active medium fills the space between mirror M₁ and lens L in Fig. 1. This restriction on the coupling implies that if only modes that are nearly identical in frequency can couple to each other, then the integer sum (m + n)must equal (m' + n').

It may be noted on this last point that the stationary states of the diffraction wave field for a single aperture correspond to a single transmission channel which is unbounded and which is guided only by the focusing



(a)

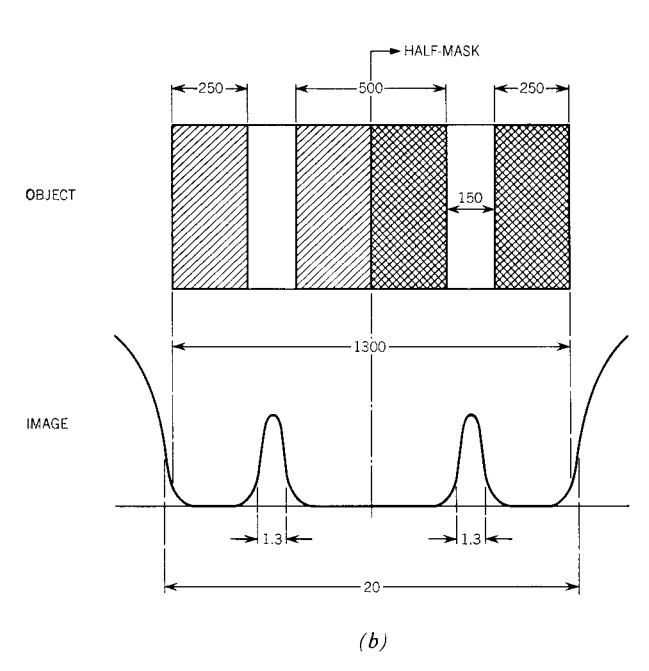


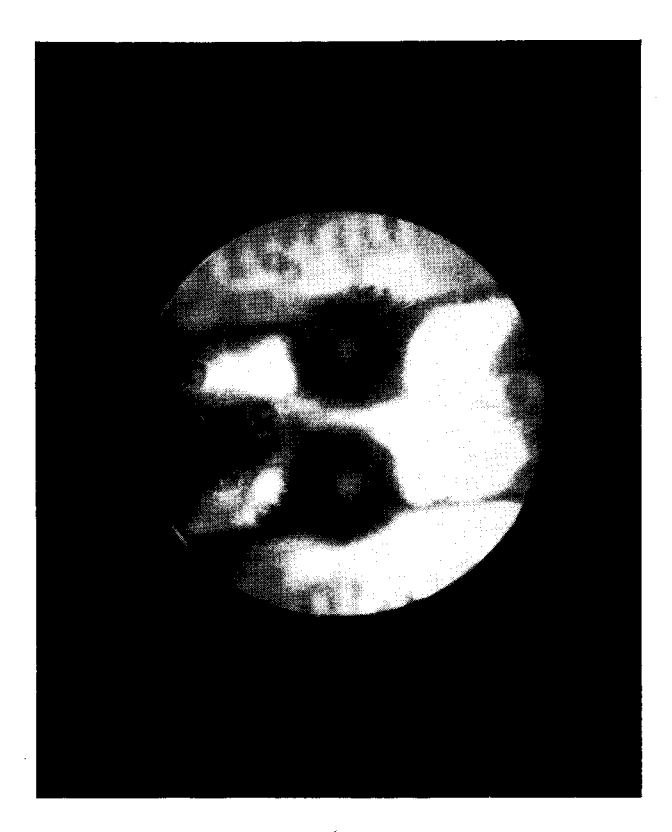
Figure 7 (a) Two parallel wires forming the half-mask object used with the apparatus of Fig. 2 to illustrate one-dimensional active imaging and (b) the image dimensions and rough intensity contours as measured in the image plane of an external objective with N.A. = 0.25, as shown in Fig. 10. All dimensions are in microns.

action of the objective of the optical cavity. The properties of this channel are otherwise analogous to those of bounded, guided wave structures such as optical fibers. If a grid consisting of a number of closely adjacent source areas is placed before M1-a mask of the type used in Fig. 3, for example—this arrangement may be regarded as a number of parallel channels that are cross-coupled through their field overlap. The requirement indicated in Eq. (36) (specifying that effective cross-coupling is achieved only for modes with the same axial mode order, q) is seen to be equivalent to a demand that the propagation constants of the coupled channels (i.e., their guide wavelengths) be identical. Similar cross-coupling can be obtained in adjacent optical fibers that are coupled through an overlapping of their fringing fields and this has been commented upon and verified by E. Snitzer.¹² This analogy is relevant here insofar as it indicates that the coherent mode coupling and mode superposition discussed here in Section 4 have well known counterparts. The active imaging system is not only self-excited, however, but the number and coupling of the adjacent channels is readily controlled by simple mask insertion.

A further consequence of the coupling term, Eq. (36), is that a mode with a large field amplitude can drive, or couple energy to, an adjacent mode even when the latter could have such a large diffraction loss that it would not independently sustain laser oscillation. The existence of this gain was demonstrated experimentally by first preparing a thin slit whose width was approximately threefourths of that required for threshold laser oscillation into this slit by itself. When a larger high-reflectivity area was then made increasingly adjacent to the thin slit it was found that oscillation in the thin slit was induced when the separation of these areas was roughly an Airy-width. The experiment was performed with the confocal system of Fig. 2; both the semimask and its conjugate image are shown in Fig. 7, together with a photograph of the image of these sources obtained from the output laser beam. If two small sections of this image, one from the region of the thin slit and one from the outer field were superimposed, stationary interference fringes were observed.

A similar experiment was conducted to examine the imaging for circular objects; in it, a small disk 750 microns in diameter with a central hole 250 microns in diameter served as the object. The resultant image is shown in Fig. 8. Although there is clear excitation of light in the central area, laser oscillation into a single hole in a large mask could not be produced unless the hole diameter was at least 550 microns. The object of Fig. 8 was supported upon a 12.5-micron wire and we note that this, too, is imaged. For both Figs. 7 and 8, the Airy width at the location of the objects is 300 microns.

In a further experiment the object consisted of two parallel wires, each 25 microns in diameter with their



(a)

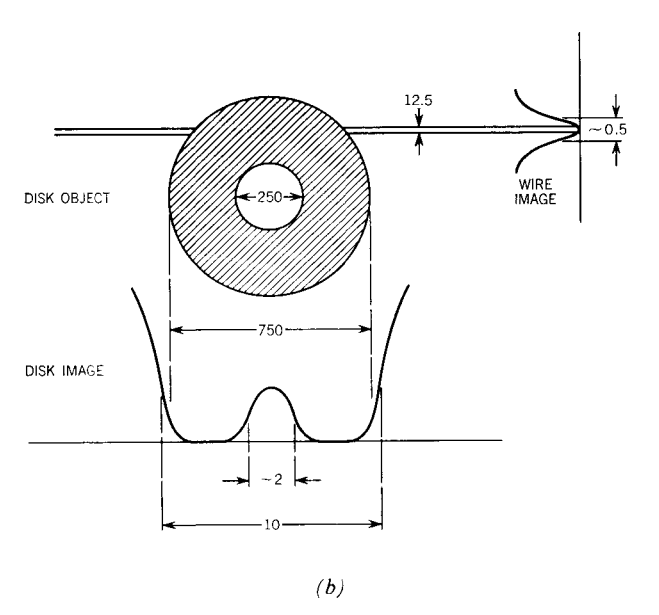


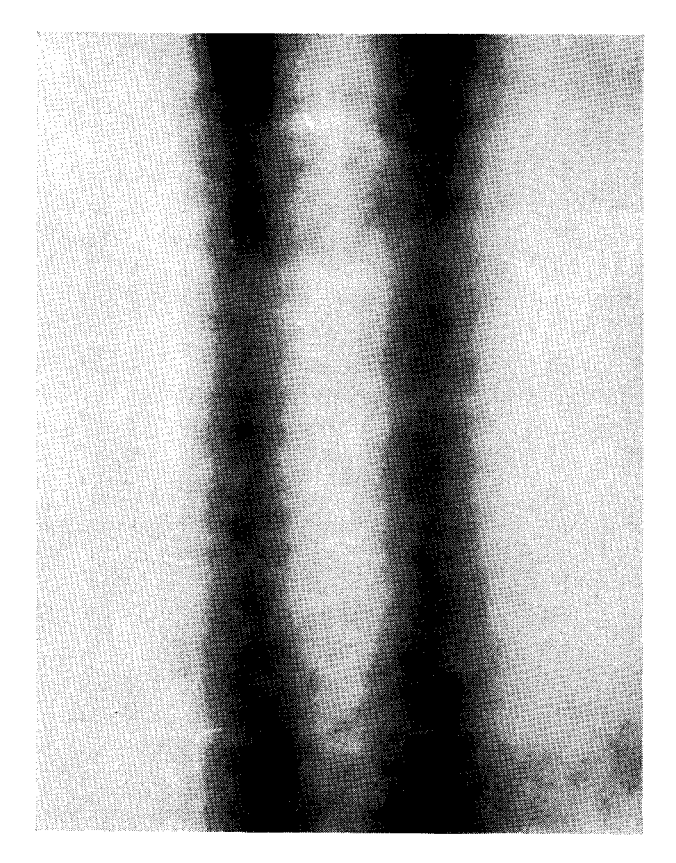
Figure 8 The disk object shown in (a) was made of 12.5-micron brass foil, supported by a 12.5-micron wire, and actively imaged with the apparatus of Fig. 2. Rough image intensity contours are sketched in (b) with the dimensions measured in the image plane of an objective with N.A. = 0.25, as shown in Fig. 10. All dimensions are in microns.

centers separated by 75 microns. The photograph of Fig. 9a (page 44) shows the image obtained when this object was placed in the laser cavity before the mirror M_1 . The same object was then illuminated by a diffraction limited laser spot of the same wavelength (6328 Å) derived from an external laser and imaged by conventional optics with an aperture diameter 5/3 greater than was used previously. The photograph of Fig. 9b indicates that the wires are just barely resolved.

It must be emphasized that the photographs in Figs. 7, 8, and 9 (obtained in active image formation) are distinctly different in their contrast and definition of detail from patterns that would be obtained in passive image formation; this difference is illustrated by the comparison photographs in Fig. 9. In passive imaging, the objects are either self-luminous or are illuminated by an external source, and the wavefields that are accepted by the imaging objective are determined solely by the conditions of illumination. Equation (6) of Section 2 expresses the diffraction spreading in the image plane of the objective lens as a superposition of the diffraction patterns from every luminous point in the object plane; it is well known that adjacent points in the resultant diffraction limited image cannot be distinguished unless the diffraction patterns at each point only partially overlap. The well known and conventional Rayleigh criterion of resolution, for example, requires that these points be separated in the image plane by one-half an Airy disk diameter, and this dimension also specifies the diffraction blurring in the image of the edge of an object.³

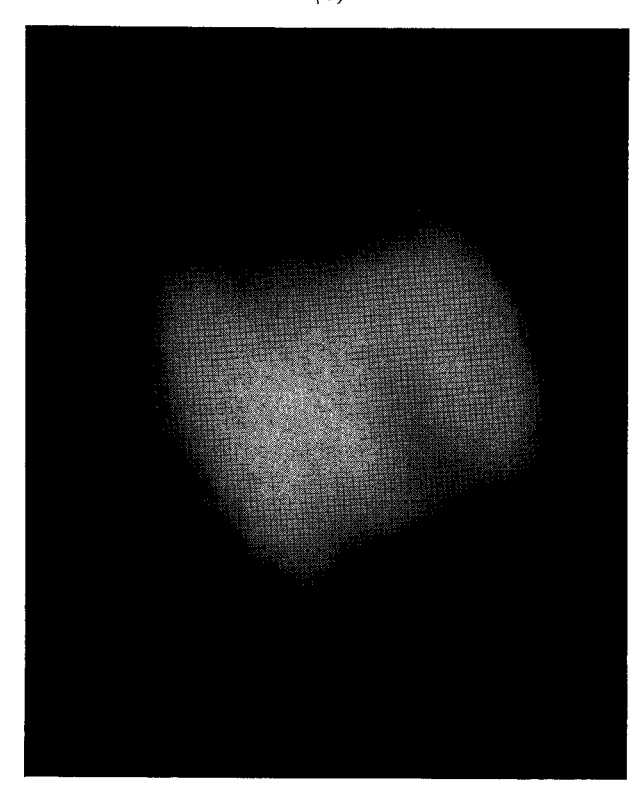
In active imaging, on the other hand, the resolution in the image is due to the contrast between the field energy in modes established in the high reflectivity areas of the control mirror M₁ and the sideband energy of the modes that spills over the object and, as has been seen, represents the diffraction loss. The significance of the superposition of low-diffraction-loss modes in active imaging, therefore, represents a capability for the cancellation of these sidebands in the resultant field distribution; the locations of the edges in the images of Figs. 7 and 8 are nearly the edges that would be observed if there were no diffraction spreading. This results, of course, from the increased contrast that follows from the sideband suppression.

Image formation in terms of such coherent superpositions was discussed over a decade ago by G. Toraldo di Francia and was considered in connection with the resolving power of an optical instrument.¹³ He was able to show that there was no theoretical limit to the resolution attainable in a local area of the optical field, and termed this process "super-resolution." That phrase is retained here, partly to differentiate active imaging as a process from conventional optical imaging techniques, and partly to indicate the attainable resolution of distinct points in the image may be considerably greater than the limit



(a)

(b)



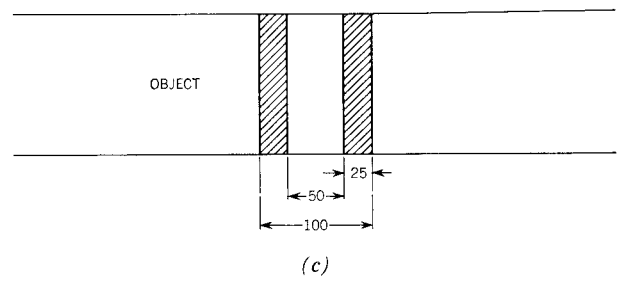


Figure 9 An object for active imaging consisting of two parallel wires. The photograph of (a) shows the intensity contrast between the wires under active imaging; that of (b) shows the intensity contrast in the image when passively imaged using a diffraction-limited spot from an external laser source as an illuminant. (The N.A. for the latter imaging was 5/3 greater than was used for the active imaging). The dimensions shown in (c), are in microns.

specified by the Rayleigh criterion.¹⁴ It may be noted, however, that when such "super-resolution" of an object or object edge has been observed in active imaging it is required that there be available a large, adjacent, high-reflectivity area at mirror M₁. In Toraldo di Francia's paper this represented an uncontrolled sideband field; in the present experiments, this expresses the demands that there be sufficient freedom for mode selection in the optical field to permit the superposition of low-diffraction-loss modes and also that the superposition can be formed to represent local detail of the perturbing obstruction or object.

Within the limits of Fraunhofer diffraction and by neglecting aberrations in the components of Fig. 1, the spatial scale of the diffraction fields at the mirrors M1 and M₂ is determined by the magnification of the system, as expressed by Eq. (3); the same scale factor will apply to images formed from the laser output beam, provided that the external optical elements used do not obstruct or vignette the field distribution. This condition is satisfied if the field distribution at the lens L of Fig. 1 or at the mirror M₂ of Fig. 2 is imaged into the clear aperture of an external objective, Le, and the field distribution in the image plane of Le then represents the magnified (or demagnified) diffraction field at the mirror surfaces of the optical cavity. This further implies that the relative scale of the fields formed within the cavity with respect to the fields in the image plane of L_e is given by the ratio of the Airy diameters for the two objectives.

Both this property and the fact that "super-resolution" in the field distribution in the active cavity is retained in subsequent passive image formation were tested experimentally with the apparatus shown in Fig. 10. L_1 is an additional lens that images the field distribution at M_2 of Fig. 2 into the aperture of L_0 . This objective was a standard microscope objective of N. A. = 0.25, and hence its Airy

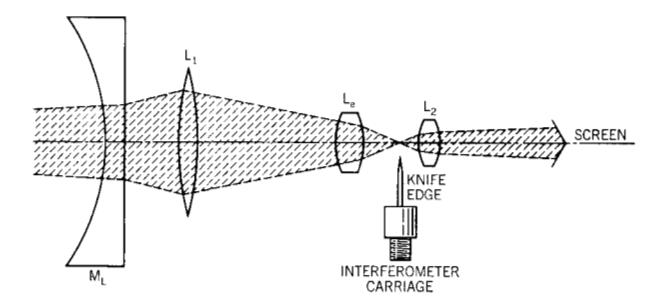
diameter for the wavelength 6328 Å is, by Eq. (1), 3.1 microns. The image formed by $L_{\rm e}$ was examined and projected by a second microscope objective, L_2 , of N. A. = 0.5. A knife edge was mounted upon an interferometer drive such that it could be traversed across the image plane of $L_{\rm e}$ to measure the scale of the diffraction in this image.

The photographs in Figs. 7 and 8 were obtained directly from the image projected by L_2 in Fig. 10. The defects in these images primarily represent lack of alignment of the objectives as well as considerable background due to dust and secondary interference fringes from the microscope objectives. The photographs were obtained with an ordinary oscillograph camera and a coarse ground glass screen; the images observed were considerably clearer and more distinct than those recorded by the photographs. The rough dimensions of the images that were determined by readings of the interferometer screw are given in these figures.

These data strongly substantiate the property of "superresolution" in active image formation. The support wire in Fig. 8, for example, is distinctly resolved and so is the edge detail in both Fig. 7 and Fig. 8, even though the conventional diffraction spread due to the lens L_e would normally be taken as greater than 1 micron. It may also be noted that these images could have been recorded directly upon a photographic film.

It is believed that the preceding discussion illustrates the origin and nature of the "super-resolution" observed in active image formation, but quantitative evaluation of the degree of resolution obtainable by this method and its dependence upon laser gain, upon the available aperture of the optical cavity, and upon the size and shape of the object cannot readily be estimated at present. To discuss this point adequately one would require, for example, a more precise measure of resolution than that given by the Rayleigh criterion. Such measurement would depend upon the contrast that can be generated by the sideband suppression of the field at image edges. An optimum solution would require the determination of

Figure 10 Apparatus used for demagnifying the laser field distribution formed at the surface of the control mirror M_1 of Figs. 1 or 2.



functions $Q_m(x)$ that satisfy Eq. (30a) with a largest eigenvalue as given by Eq. (32), noting that the range of integration in Eqs. (30a) and (32) is over multiple-source areas.

If $Q_m(x)$ is expanded in terms of known functions, as in Eq. (29), the restrictions discussed after Eq. (36) indicate that the functions of the expansion must have the same order, m, because only such functions can cross-couple to produce a time-stationary field distribution. This type of coupling was assumed in the two-slit example given at the beginning of this Section, but this example was highly illustrative—it cannot be assumed that the optimum field distributions at each slit are eigenfunctions of the slit of width $(b-\delta)$ or that such functions would remain centered on the assumed central position x_0 ; or, if the interval $(b-\delta)$ is large, that other eigenfunctions of the same order and also of low diffraction loss could not be added to yield a lower net diffraction loss. That is, if the field is to be represented by the sum

$$Q_m(x) = \sum_{i=1}^t a_i U_m^{c_i}(x - x_0^i)$$
 (37)

for a given object distribution at mirror M_1 , and a solution of $Q_m(x)$ is sought that satisfies Eq. (30a) and yields a maximum eigenvalue σ_m , 3t+1 parameters must be determined; i.e., t itself and the 3t adjustable parameters a_i , c_i , and x_0^i . And, of course, even if this eigenfunction were determined, it would not be expected to be an eigenfunction with respect to Eqs. (24) representing the interaction of this mode with the active medium.

5. Conclusions

The field distributions that have been generated in the experiments reported here have been controlled by the physical insertion of masks or objects into the optical cavity, but a more general and more rapid control can be obtained by the selection of individual high reflectivity spots at a control surface through the use of a raster of electro-optically controlled elements acting as switches. A summary analysis of such a device acting as a laser character projector has been reported elsewhere, but one special advantage obtains from the insertion of the control elements directly into the laser cavity, resulting in a minimum control energy requirement for optical spot selection.15 This reflects both the fact that the cross-sectional area of the switch is determined as a diffraction-limited dimension of the laser cavity and the requirement that the inserted loss need only be sufficient to suppress laser oscillation into the switch area. A prototype of such a projector has been constructed and tested experimentally; the results support and provide a specific evaluation of the power efficiency of this type of optical control.

With the gas laser operating in the visible transition,

the minimum single-aperture diameter is about 2.5 Airy disk diameters or 0.06 cm for one-meter spacing between mirror and objective. The full available aperture that corresponds to a 0.7-cm inner diameter discharge tube is found to be less than this, but can be as large as 0.6 cm. An upper limit for the number of individual high-reflectivity areas that can be established at a control mirror surface is thus 10×10 , although in this limit there is considerable field overlap and the laser oscillation within these parallel channels is strongly coherently coupled. Rasters of individual spots formed by grids ranging from 6×6 to 8×8 spots have been used in character formation, as indicated in Fig. 3.

This limitation in the number of attainable spots of course reflects the low gain and the long and narrow discharge tubes of the helium-neon gas laser. It is expected that systems in which the depopulation of the terminal state of the laser transition does not depend on wall collisions would allow active imaging with considerably larger diameters of the active medium and would have larger optical apertures, permitting increases either in the number of individual spots used in image formation or in the detail available in "super-resolution" as discussed in Section 4. The recently announced H_{θ}^+ gas laser shows great potential for this application; solid state lasers of high optical homogeneity such as the neodymium glass laser would also permit very large apertures to be achieved, although they would require pulsed operation. ¹⁶

It is recognized that the research reported in this paper is preliminary in character, but it is believed that the present experiments demonstrate the technical potential of active imaging and illustrate the nature of this process as it originates in the interaction between the degenerate modes of the optical cavity and the active medium. These techniques should find application in microscopy and in the reading and writing of high bit density information, but it would be premature to speculate on these applications at the present time. This work does raise general questions that are beyond the scope of this paper, especially questions as to the nature and degree of resolution that can be realized in optical image formation.

Acknowledgments

The author acknowledges with pleasure the interest and the comments of Drs. N. Braslau, G. Lasher, A. Nethercot, D. Jhirad, and R. Pole. Additionally, he wishes to express his appreciation to Professor E. Wolf who graciously read and made extensive suggestions concerning an early draft of this paper. The material presented herein is, however, entirely the author's responsibility.

Footnotes and references

- 1. C. Townes and A. Schawlow, Phys. Rev. 112, 1940 (1958).
- W. Wagner and G. Birnbaum, J. Appl. Phys. 32, 1185 (1961).
- M. Born and E. Wolf, Principles of Optics, Pergamon Press, London and New York, 1959, Chapter IX.
- 4. A. G. Fox and T. Li, Bell System Tech. J. 40, 453 (1961).
- G. Boyd and J. Gordon, Bell System Tech. J. 41, 1371 (1961).
- 6. R. Soohoo, Proc. IEEE 51, 70 (1963).
- 7. E. Wolf, Phys. Lett. 3, 166 (1963).
- 8. Several recent papers have discussed optical cavities that employ multiple optical elements and are similar to the cavity discussed in this paper. These include "Analysis of Optical Resonators Involving Focusing Elements" by S. A. Collins, Jr., in Applied Optics 3, 11 (1964), and "Conjugated-Concentric Solid-State Laser System" by R. V. Pole, Paper GB-13, Bull. Amer. Phys. Soc., (January 1964) and to be published in J. Opt. Soc. Am. In his paper, "Laser With a Multihole Diaphragm" T. Morokuma (Journal of Research, NBS, 68C, 25 (1964)) uses a laser cavity that is essentially identical with Fig. 2 of this paper, but does not relate his work to the imaging property of this cavity. His observations on the standing wave pattern formed on the objective mirror M2 of Fig. 2 are pertinent to the present paper.
- D. Slepian and H. O. Pollak, Bell System Tech. J. 40, 43 (1961).
- 10. W. R. Bennett, Jr., Phys. Rev. 126, 580 (1962).
- C. L. Tang, H. Statz, and G. DeMars, J. Appl. Phys. 34, 2289 (1963).
- 12. E. Snitzer, Advances in Quantum Electronics, Columbia University Press, New York, New York, 1961, p. 348.
- 13. G. Toraldo di Francia, Suppl. Il Nuovo Cimento 9, 426 (1952).
- 14. W. A. Hardy, Nature 202, 277 (1964).
- 15. W. A. Hardy, IBM Report NC-350, December 1963.
- 16. W. E. Bell, Appl. Physics Letters 4, 34 (1964).

Received March 17, 1964 Revised manuscript received July 13, 1964